Single plasmon spatial and spectral sorting on a crystalline two-dimensional plasmonic platform

Upkar Kumar,[1] Sreenath Bolisetty,[2] Raffaele Mezzenga,[2] Christian Girard,[1] Erik Dujardin,[1] and Aurélien Cuche[1]

[1] CEMES, University of Toulouse and CNRS (UPR 8011), 9 rue Jeanne Marvig, BP 94347, 31055 Toulouse, France

[2] ETH Zurich, Department of Health Sciences and Technology, Schmelzberg-strasse 9, CH-8092 Zurich, Switzerland

* Corresponding author: aurelien.cuche@cemes.fr

Supplementary information

Table of contents

S1. Contribution of parasitic luminescence from gold

When excited in the visible, gold exhibit a broad luminescence that originates from internal electronic recombination. This well-documented phenomenon might be problematic in quantum plasmonic experiments where the number of photons involved is extremely low. In order to quantify the effect of this parasitic luminescence, we have positioned the laser spot at several locations directly on top of the flake and compared the intensity of the signal to the reference recorded on the nanodiamond. The results presented in Figure S1 confirm that the parasitic signal at the launching point is weak compared to the NV signal. Moreover, while SP-mediated delocalization of the signal can be observed for excitation on the diamond, nothing is observed in the case of direct excitation on gold. These results confirm the dominant contribution of the single plasmons launched by the quantum source, as discussed in the main manuscript.

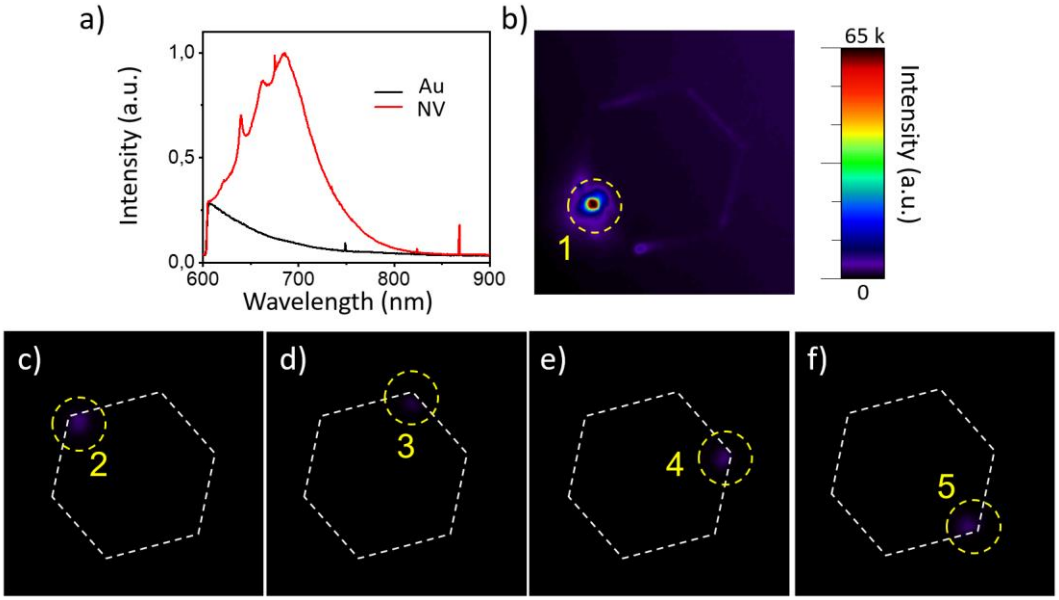

Figure S1. (a) Luminescence spectra from the NV^- center, recorded at position 1 directly on the nanodiamond, and from gold acquired when the excitation spot is parked at position 2. The purple area gives a qualitative picture of the offset induced by the parasitic luminescence from gold. (b-f) Serie of wide-field luminescence images acquired for different positions of the laser excitation on the pristine flake. The positions of the excitation laser are indicated by the yellow dashed circles.

S2. Local electric field at excitation wavelength (λ=532 nm)

The measurements of intensity on the nanodiamond or along the perimeter of the gold flake have shown really small variations when the polarization of the incident excitation laser is rotated. This behavior can be understood if the transition dipole at absorption is mainly oriented along the z-axis.

Normally, a z dipole would hardly be excited by a polarization lying in the xy plane. But the depolarization induced at the edge of the flake (where the ND is positioned) might explain this behavior. We have simulated the distribution of the total electric field intensity along with the vectorial field distribution of the scattered field in the xz plane for two orthogonal polarizations. The results are presented in Figure S2 and it already gives part of the answer concerning the efficient excitation of the NV center since an important depolarization is observed in the vicinity of the edge of the flake, with a non-zero z-component of the electric field.

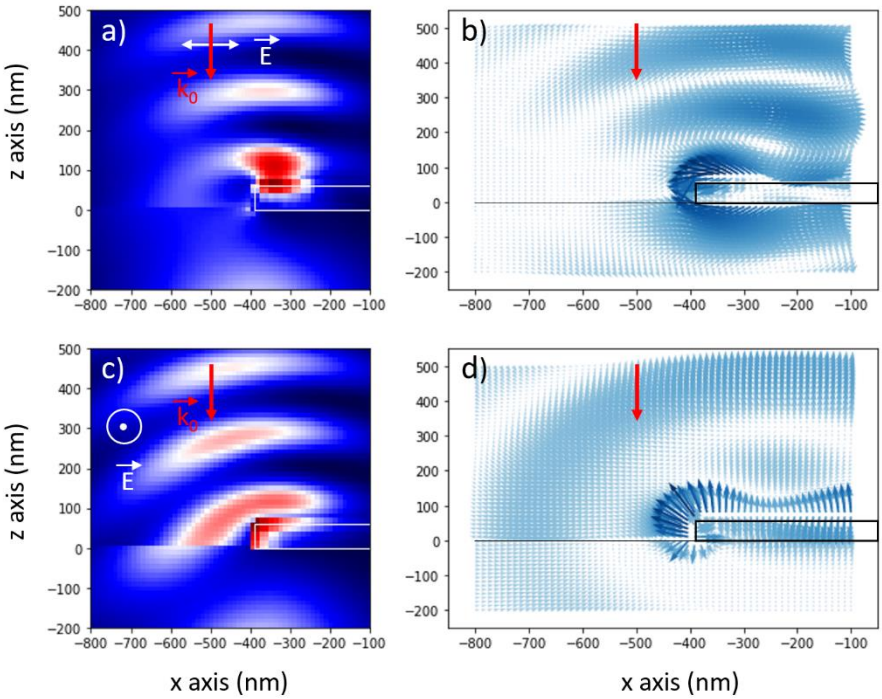

Figure S2: Depolarization at the edge of the flake. Simulated intensity of the total electric field (incident + scattered by the structure) in the xz plane at the excitation wavelength (λ=532 nm) for an incident polarization (a) along x (0°) or (c) along y (90°). The gold flake is delimited by the white contour. The incident polarization is indicated by the white arrow, while the red one indicates the incident wavevector. Corresponding vectorial field map only for the scattered contribution for an incident polarization (b) along x (0°) or (d) along y (90°).

S3. Simulations of signal transfer for different dipole orientations: z-dipole vs "scalar" source

The simulations of signal transfer presented in the main manuscript correspond to the incoherent sum of three simulated maps for dipolar sources oriented along the x, y and z-axis respectively, and this for a given wavelength. The Figure S3 shows the intermediate simulated maps for each dipole orientation and the resulting incoherent sum at a wavelength of λ=700 nm.

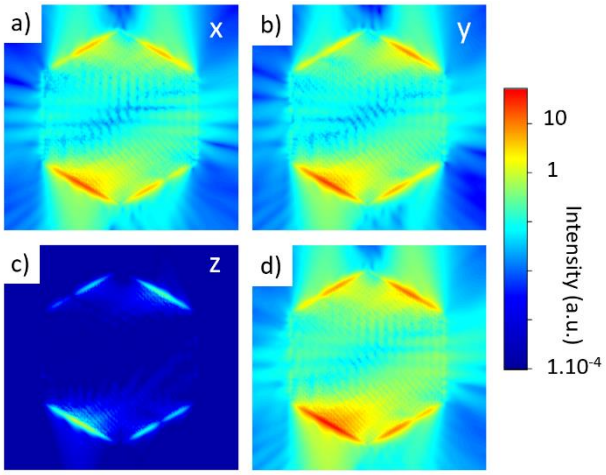

Figure S3: Simulated signal transfer maps in the two-dimensional gold flake for the three dipole orientations at λ=700 nm. (a) Dipole oriented along the x-axis. (b) Dipole oriented along the y-axis. (c) Dipole oriented along the z-axis. (d) Simulated image with a "scalar" source, corresponding to the mean of the simulated maps in (a-c).

Because of the uncertainty on the orientation of the transition dipole associated to the NV center, the simulated transfer maps in the main manuscript have systematically presented as the incoherent mean of images computed for three orthogonal dipoles. However, assuming that the excitation and emission dipoles associated to the NV center are aligned and mainly along the z-axis, presenting only the simulated transfer maps for a z dipole might be an alternative. Figure S4 presents the comparison between the two approaches for the five wavelengths investigated in the main manuscript. These two types of images lead to quasi-similar distributions of the electric field above the flake (but with different intensities). These results validate our approach where the mean of the three image is used.

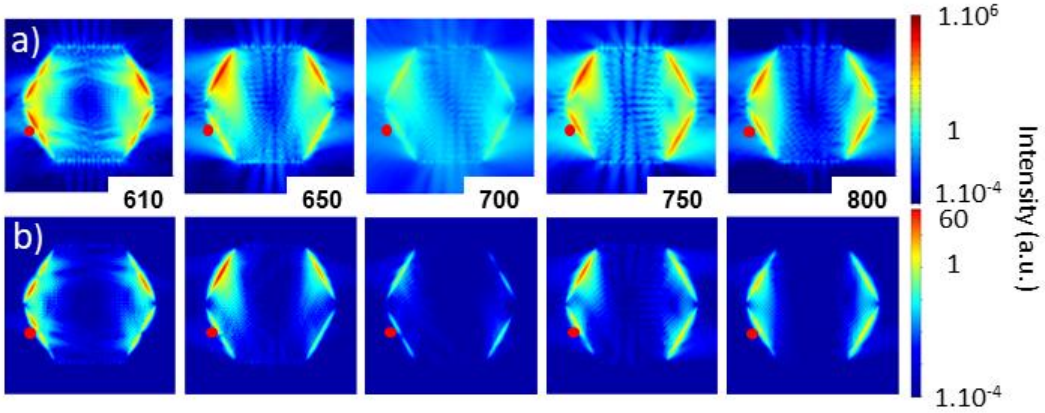

Figure S4: Comparison of simulated signal transfer maps in the two-dimensional gold flake (a) for the incoherent sum of three maps computed for the three orientations of the dipole (along x, y and z) (b) and for a dipole along z alone, at the five different wavelengths (from left to right: λ= 610, 650, 700, 750 and 800 nm). The position of the dipolar emitter is indicated by a red dot.

S4. Hyperspectral luminescence wide-field maps of the drilled flake (Bragg mirror)

The Figure S5 presents the discrete spectral decomposition of the image presented in the Figure 3(d) of the main text. For this purpose, five narrow bandpass filters centered at λ_{bp}=610, 650, 700, 750 and 800±10 nm respectively, have been used.

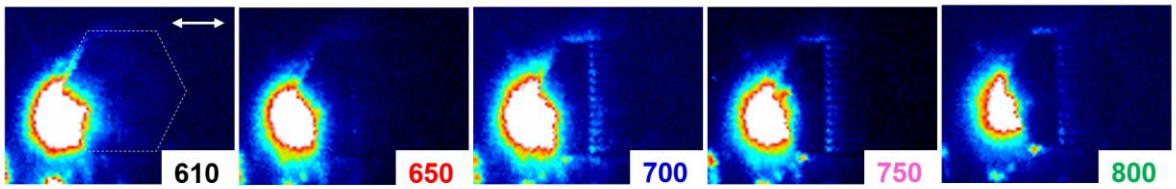

Figure S5. Serie of wide-field luminescence images acquired at five different wavelengths on the flake redesigned with the hole array. From left to right: bandpass filters are centered at λ_{BP} = 610, 650, 700, 750 and 800 nm. The white arrow indicates the laser polarization at 0°.

S5. Simulated signal transfer for a flake made of silver

As discussed in the main manuscript, because of the wavelength-dependent Ohmic losses, the propagation in plasmonic metals already acts as a spectral filter. It is therefore possible to consider different plasmonic materials to tune this damping effect. For instance, the Figure S6 shows that the same structure made of silver would be a good alternative at the shortest wavelengths emitted by the NV center (λ=600 nm), since an efficient signal transfer is observed for the three dipole orientations considered in this work.

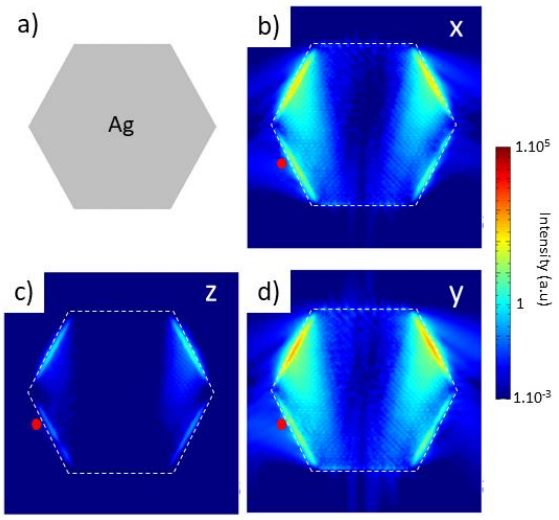

Figure S6. Simulated signal transfer maps in a two-dimensional silver flake with similar dimensions as the gold one studied in this work, for the three dipole orientations at λ=600 nm. (a) Scheme of the mesh reproducing the geometry of a silver flake. (b) Dipole oriented along the x-axis. (c) Dipole oriented along the z-axis. (d) Dipole oriented along the y-axis.

S6. Effect of the thickness of the flake on the propagation of SPP

We discuss here the effect of the thickness of the plasmonic structure on the wavelength-dependent propagation of the plasmons. Because of computation time limitation, we computed the intensity of the electric field at the right extremity of a plasmonic gold wire as a function of both the wavelength and the thickness. The length of the wire is 1 µm and the width is 200 nm. On the other hand, the altitude of the emitter is kept constant at 27.5 nm. We choose three thicknesses h=20, 60 and 100 nm that are representative of plasmonic structures described in the literature.

Although the results cannot be directly translated to the flake since the geometry is different, the results of the numerical experiment presented in Figure S7 provide interesting insight into the coupling between the scalar emitter (averaged incoherent sum of three dipoles) and the plasmonic structure. It shows that the transmission efficiency is relatively homogeneous. Only a peak in the transmission is observed at 700 nm (h=60 and 100 nm) or 750 nm (h=20 nm) that may result from resonant conditions in the wire. Therefore, the thickness of the structure does not affect drastically the coupling between the emitter and the structure and is not a critical parameter.

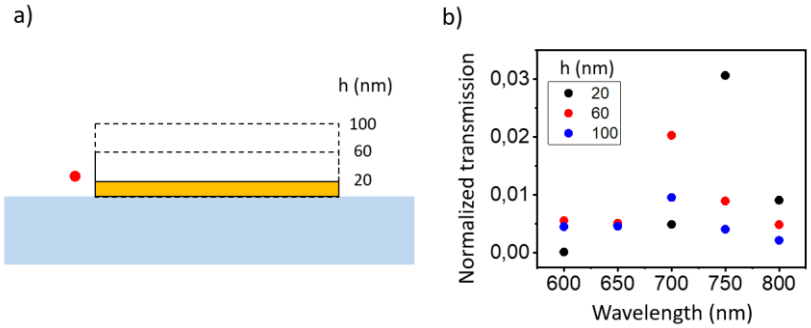

Figure S7. (a) Geometry of the simulated system. A "scalar" emitter is located at a fixed position at the entrance of a 1 µm-long rectangular gold wire. The width of the wire is 200 nm, and the height is varied (h= 20, 60 or 100 nm). (b) Simulated normalized signal transfer 30 nm above the right extremity of the wire presented in (a) as a function of the thickness of the guide.

S7. Effect of the position of the emitter with respect to the flake

The figure S8 shows the effect of the emitter on the signal distribution 30 nm above the gold flake. These simulations have been computed at a single wavelength λ=750 nm. The two images have the same scale as Figure 5 in the main text for direct comparison. These maps reveal that the spatial distribution of the signal in the hexagonal structure is quite robust with respect to the emitter position. Indeed, only slight modifications of the pattern and the local intensity are observed. This may be due to the boundaries of the flake and interferential effects that constrain the scattering along preferential edges of the structure.

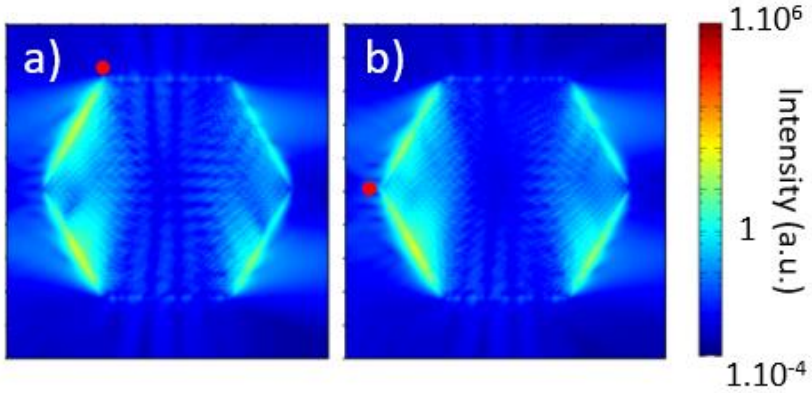

Figure S8. (a-b) Simulated signal transfer maps in a two-dimensional gold flake for two different positions of the scalar emitter at λ=750 nm.